

Supplementary Information

High-Performance n-type Polymer Field-effect Transistors with Exceptional Stability

Manikanta Makala¹, Maciej Barlög², Derek Dreman¹, Salahuddin Attar², Edgar Gutiérrez Fernández^{3,4}, Mohammed Al-Hashimi^{5*}, Oana D. Jurchescu^{1*}

¹Department of Physics and Center for Functional Materials (CFM), Wake Forest University, Winston Salem, NC 27019, USA.

²Department of Chemical Engineering, Texas A&M University at Qatar, P.O. Box 23874, Doha, Qatar.

³Department of Physics, University of Warwick, Gibbet Hill Road, Coventry, CV4 7AL, UK.

⁴XMas/BM28-ESRF, 71 Avenue Des Martyrs, F-38043 Grenoble Cedex, France.

⁵College of Science and Engineering, Hamad Bin Khalifa University, P.O. Box: 34110, Doha, Qatar.

*Corresponding authors: jurchescu@wfu.edu, Malhashimi@hbku.edu.qa

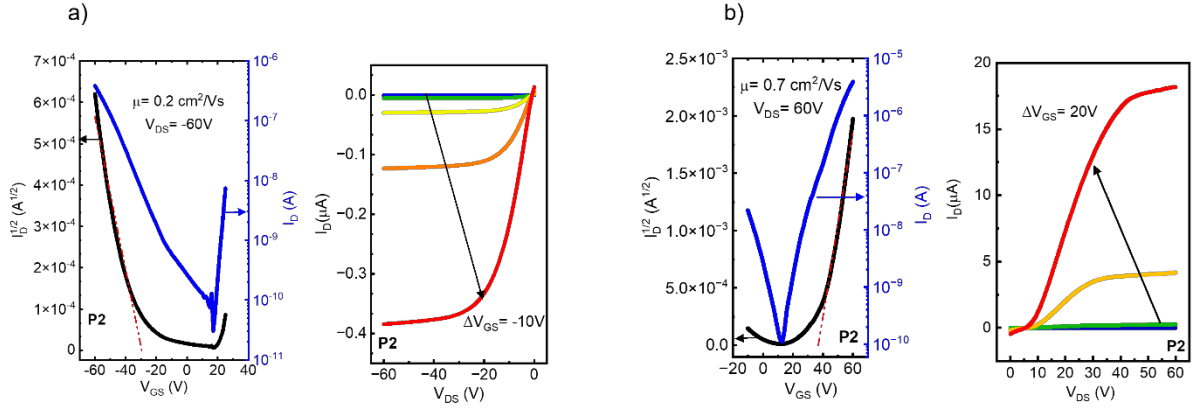


Figure S1. Transfer and output characteristics of a p-type OFETs based on P2. Here L/W= 50/400 (a), transfer and output characteristics of n-type OFETs based on P2. Here L/W= 40/800 (b).

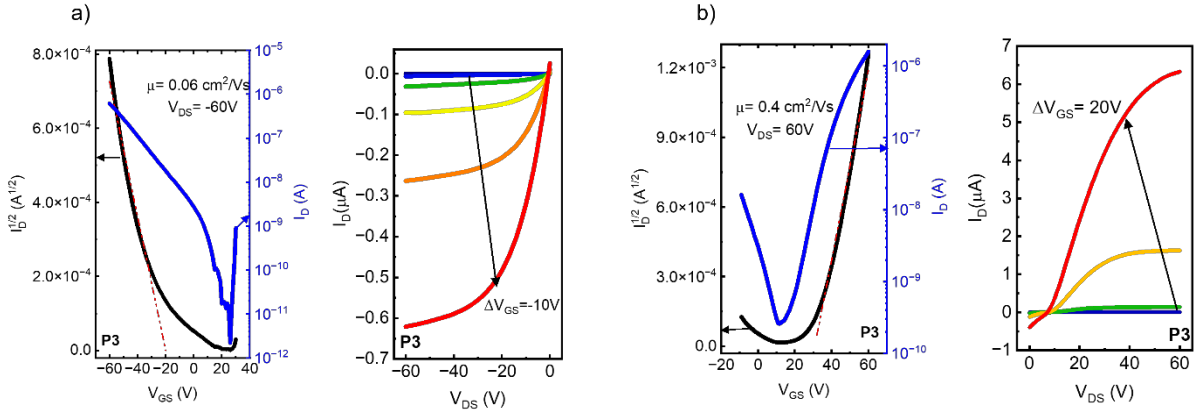


Figure S2. Transfer and output characteristics of a p-type OFETs based on P3. Here L/W= 30/400 (a), transfer and output characteristics of n-type OFETs based on P3. Here L/W= 40/400 (b).

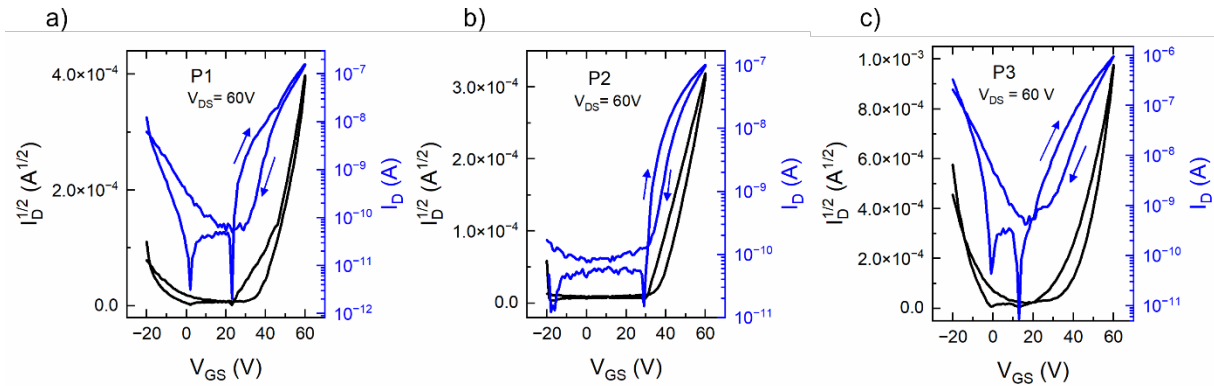


Figure S3. Hysteresis in transfer characteristics of a n-type OFETs based on polymers P1 (a), P2 (b), P3 (c).

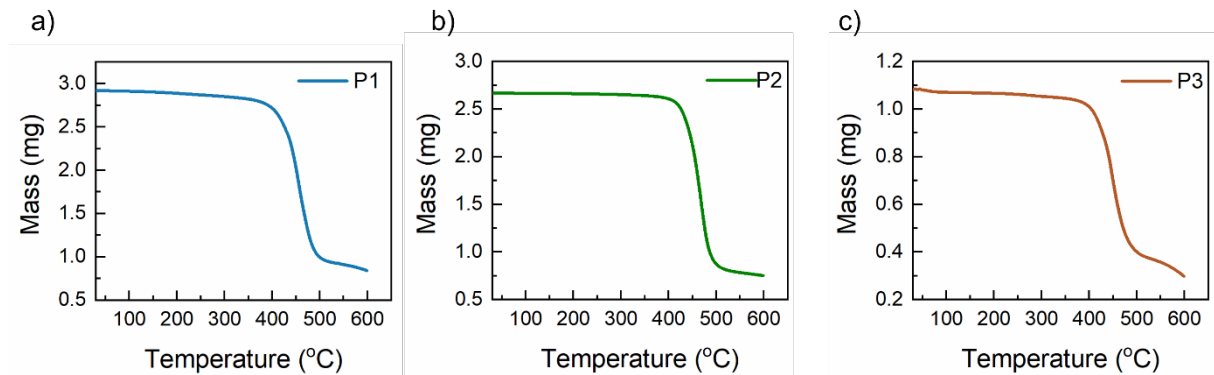


Figure S4. Thermogravimetric analysis (TGA) curves of polymers P1 (a), P2 (b), P3 (c). The decomposition temperatures (T_d) corresponding to 5% mass for polymers P1, P2 and P3 are 384 °C, 421 °C, and 386 °C, respectively.

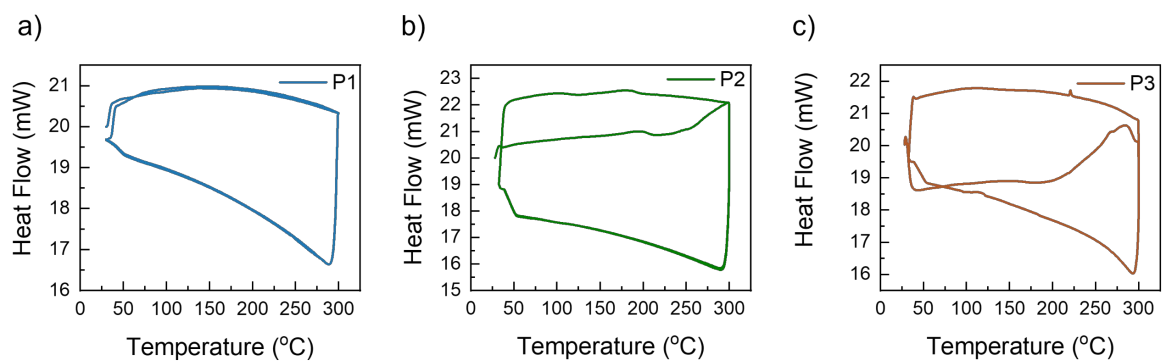


Figure S5. Differential scanning calorimetry (DSC) thermograms of polymers P1 (a), P2 (b), P3 (c).

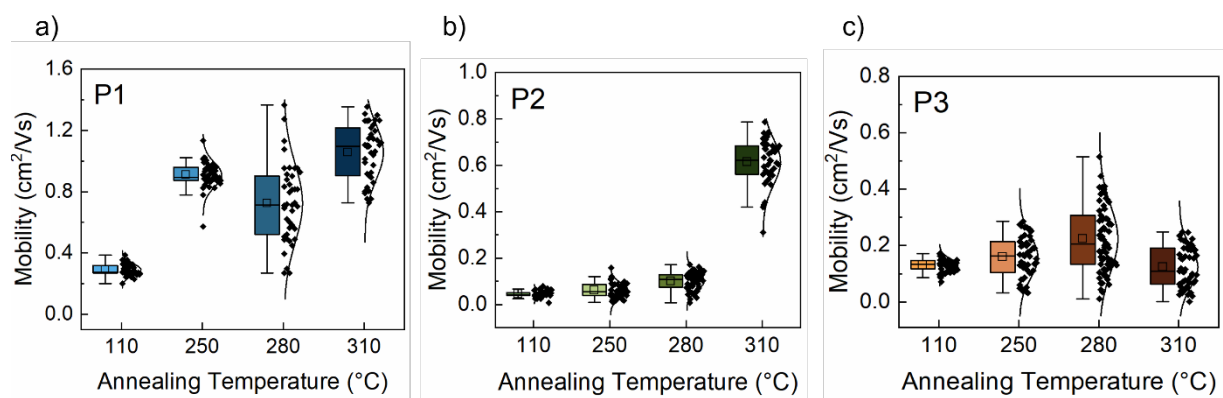


Figure S6. Mobility values for the n-type OFETs fabricated on polymer films that were annealed at temperatures ranging from 110 °C to 310 °C for P1 (a), P2 (b), and P3 (c).

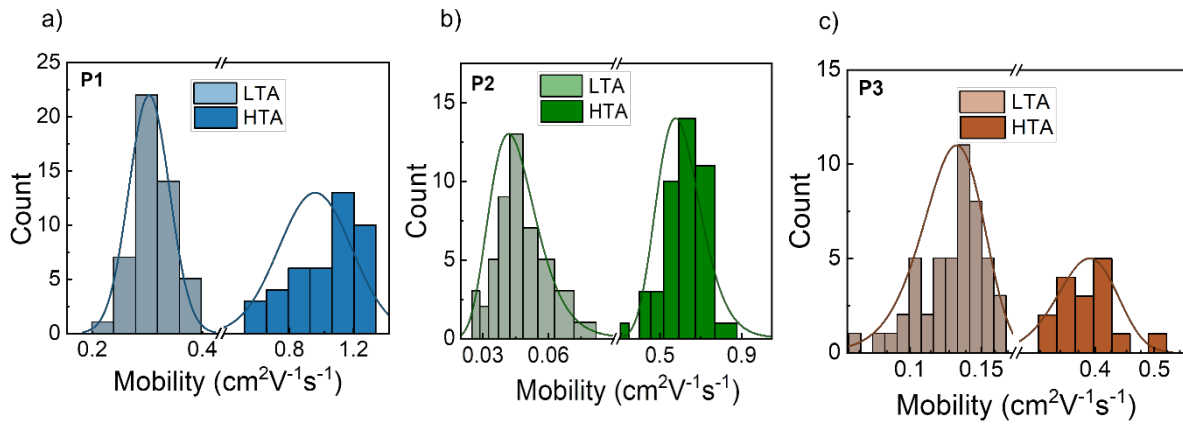


Figure S7. Mobility histograms of n-type OFETs based on polymer films annealed at low temperature (LTA) and high temperatures (HTA) for P1 (a), P2 (b), and P3 (c).

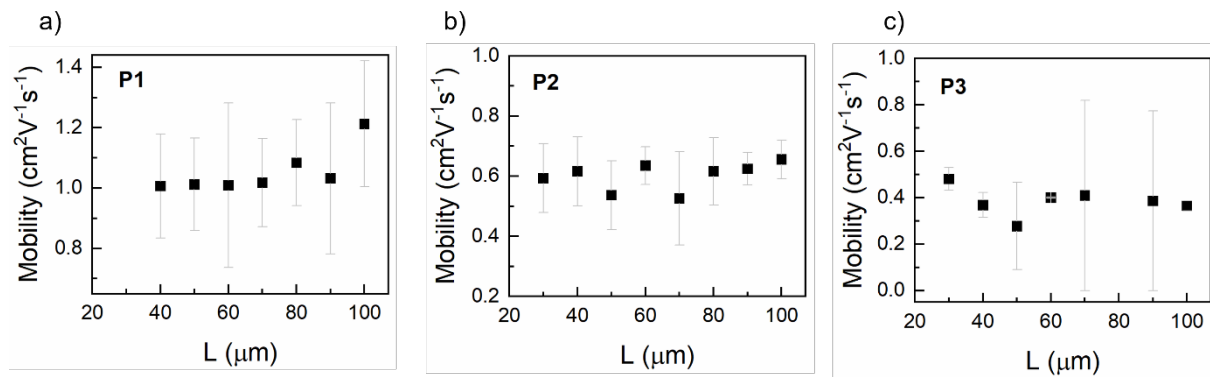


Figure S8. Channel length dependence of electron mobility for P1 (a), P2 (b), and P3 (c).

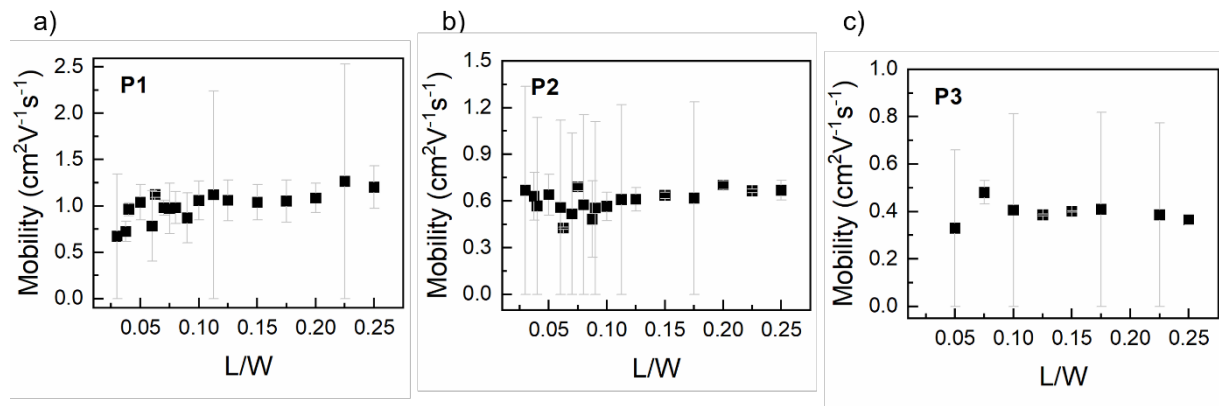


Figure S9. Dependence of electron mobility on width normalized channel length for P1 (a), P2 (b), and P3 (c).

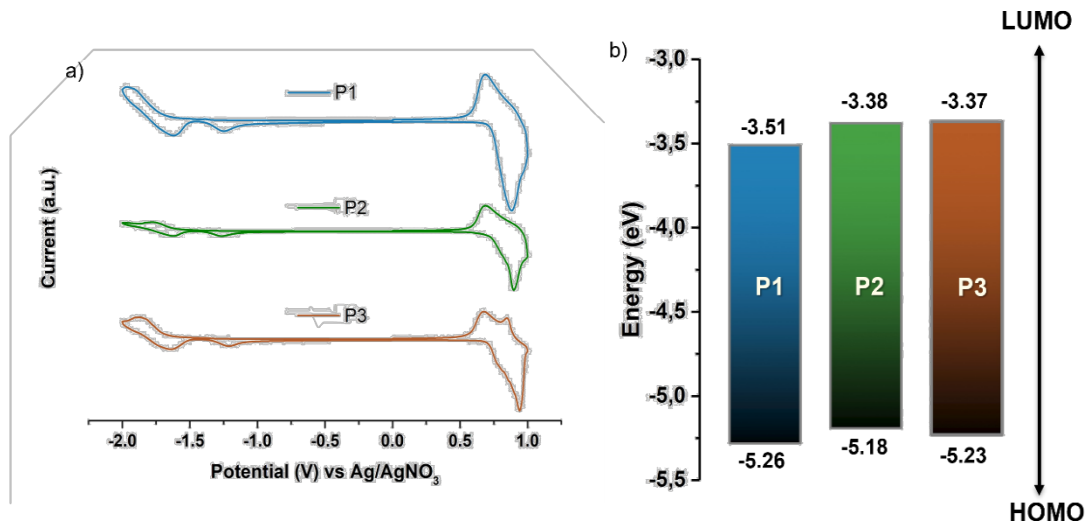


Figure S10. Cyclic voltammograms of P1–P3 films on a glassy carbon electrode measured in a $0.1 \text{ mol L}^{-1} \text{Bu}_4\text{N}^+\text{PF}_6^-$ acetonitrile solution at a scan rate of 0.1 V s^{-1} ; (b) energy-level diagram for P1–P3 according to CV measurements.

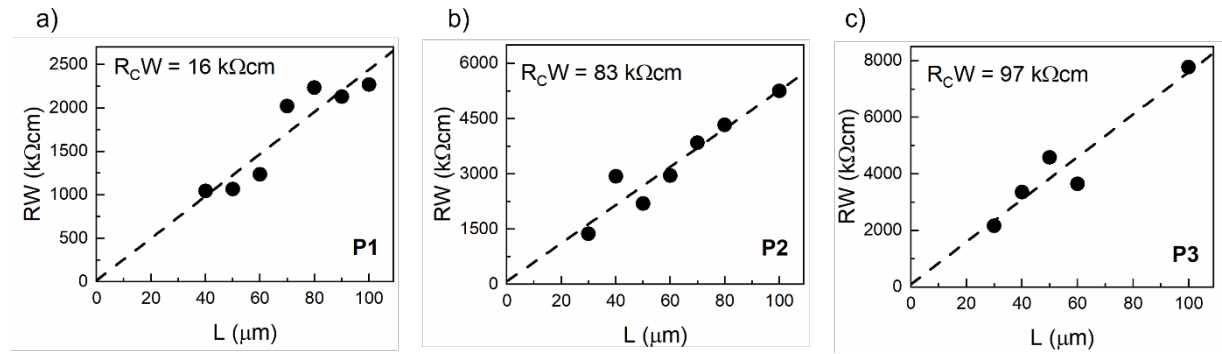


Figure S11. Width-normalized total OFET resistance plotted as a function of channel length L in n-channel OFETs based on P1 (a), P2 (b), and P3 (c).

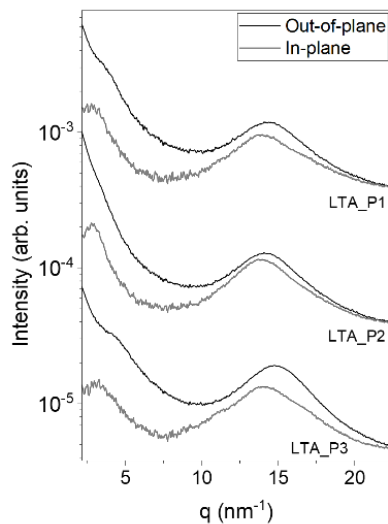


Figure S12. Azimuthal integrations of the GIWAXS patterns along the q_z axis(out-of-plane) and along the q_r axis (in-plane).

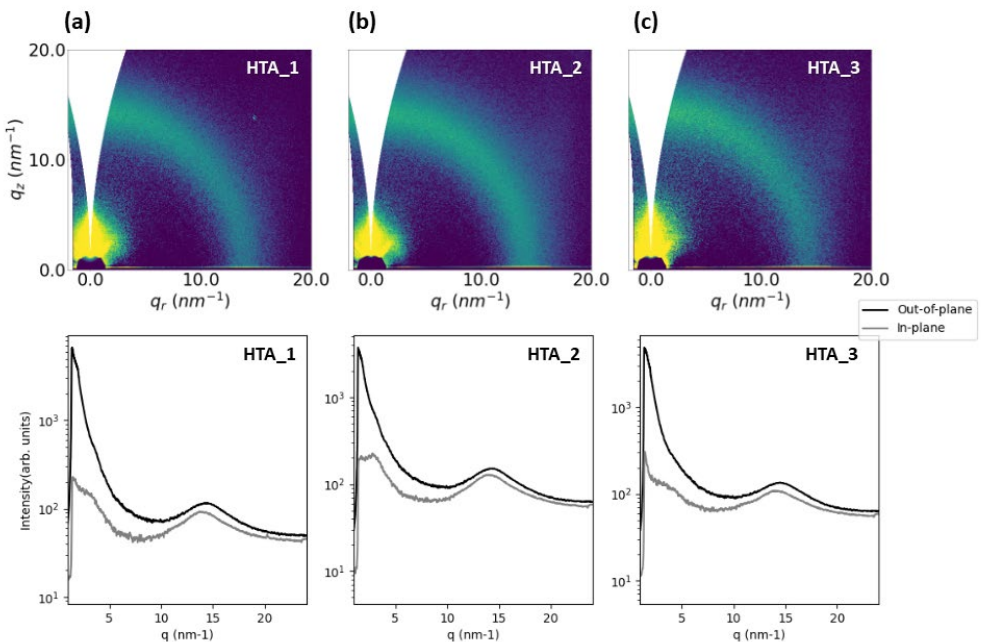


Figure S13. Upper row: 2D scattering GIWAXS patterns acquired on films of polymers P1 (a), P2 (b), P3 (c) annealed at high temperatures. Bottom row: corresponding azimuthal integrations of the GIWAXS patterns along the vertical (out-of-plane) and horizontal (in-plane) axis.

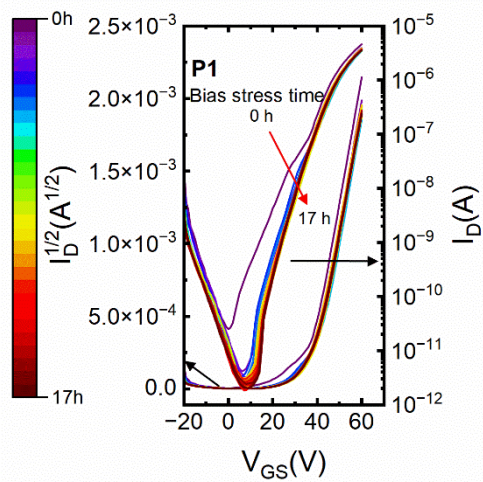


Figure S14. Transfer curves measured on OFETs of P1 films annealed at high temperatures (HTA) during 17h of continuous bias stress at $V_{GS} = V_{DS} = 60\text{V}$.

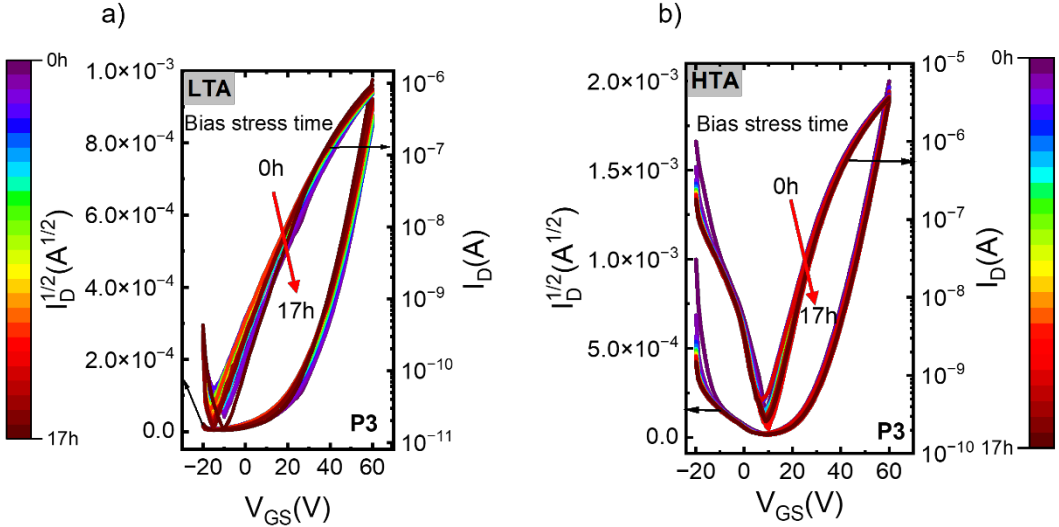


Figure S15. a) Transfer curves measured on OFETs of P3 films annealed at low temperatures (LTA) during 17h of continuous bias stress at $V_{GS} = V_{DS} = 60\text{V}$. b) Transfer curves measured on OFETs of P3 films annealed at high temperatures (HTA) during 17h of continuous bias stress at $V_{GS} = V_{DS} = 60\text{V}$.

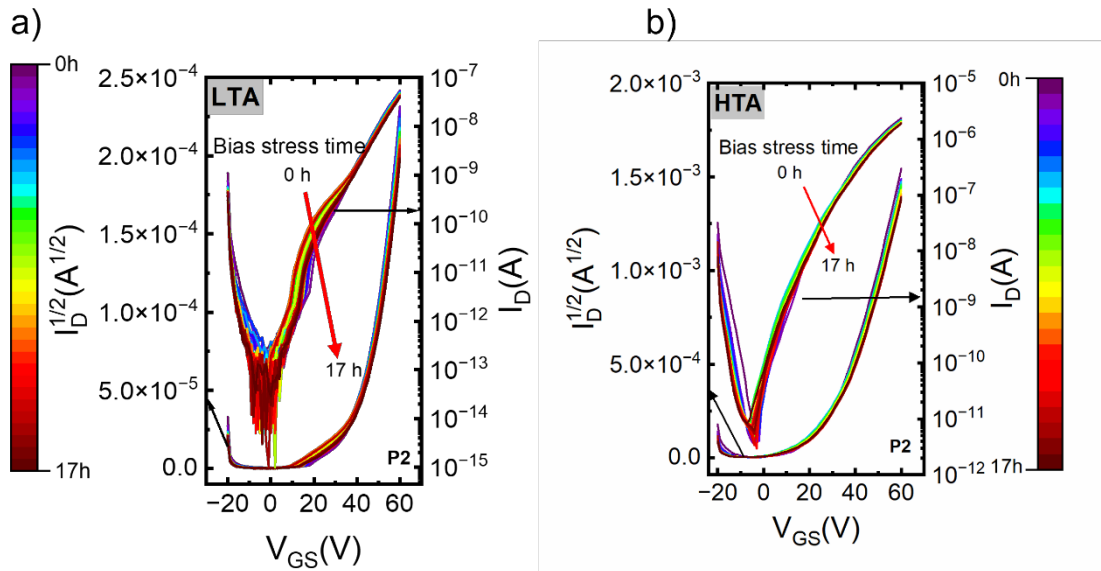


Figure S16. a) Transfer curves measured on OFETs of P2 films annealed at low temperatures (LTA) during 17h of continuous bias stress at $V_{GS} = V_{DS} = 60\text{V}$. b) Transfer curves measured on OFETs of P2 films annealed at high temperatures (HTA) during 17h of continuous bias stress at $V_{GS} = V_{DS} = 60\text{V}$.

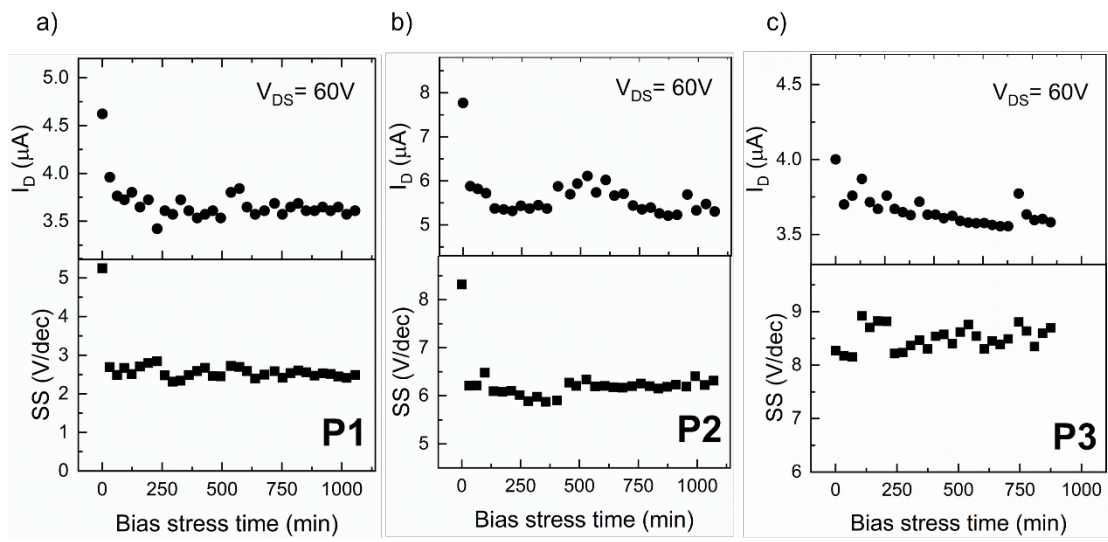


Figure S17. Evolution of drain current and subthreshold slope with time for n-type OFETs upon continuous bias stress at $V_{GS}= V_{DS}= 60\text{V}$ based on P1 (a), P2 (b), and P3 (c).

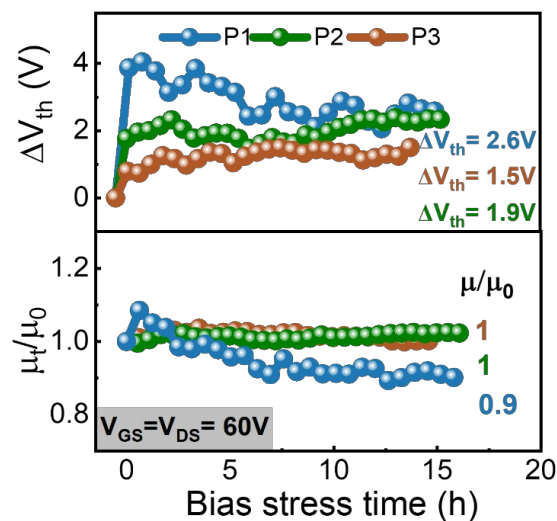


Figure S18. a) Evolution of ΔV_{th} and mobility with stress time for n-type OFETs upon continuous bias stress at $V_{GS}= V_{DS}= 60\text{V}$ based on polymer annealed at high temperatures.

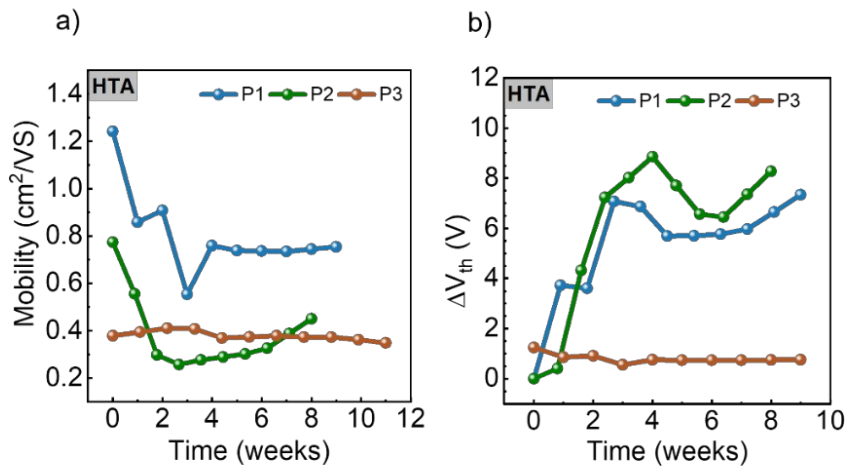


Figure S19. Shelf-life study on three polymers with minimum exposure to humidity: evolution of μ (a), and ΔV_{th} (b). The samples were stored in an amber-colored desiccator at room temperature under 750 torr between measurements. The devices were exposed to the ambient atmosphere during transfer to the probe station.

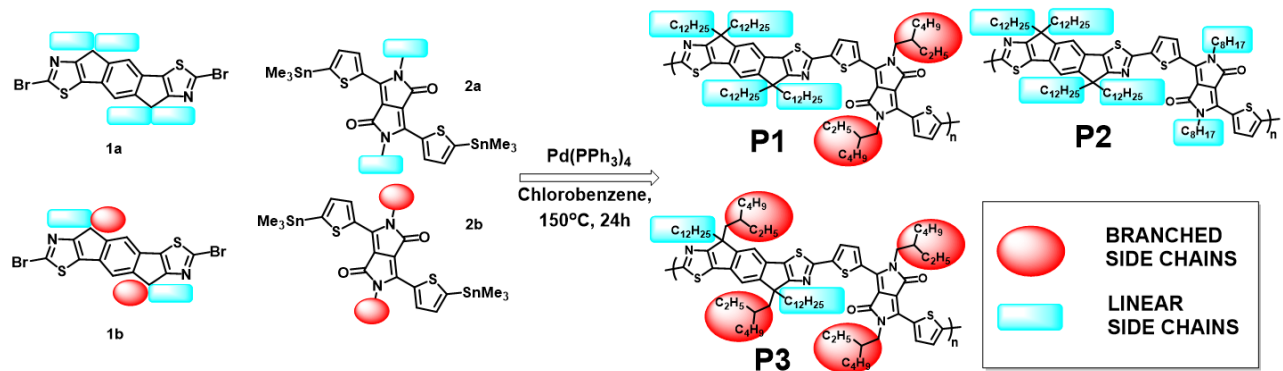


Figure S20. Chemical structures of IDTz-DPP polymers with alkyl sidechain engineering. The branched and linear sidechains are highlighted with red and blue highlights, respectively.

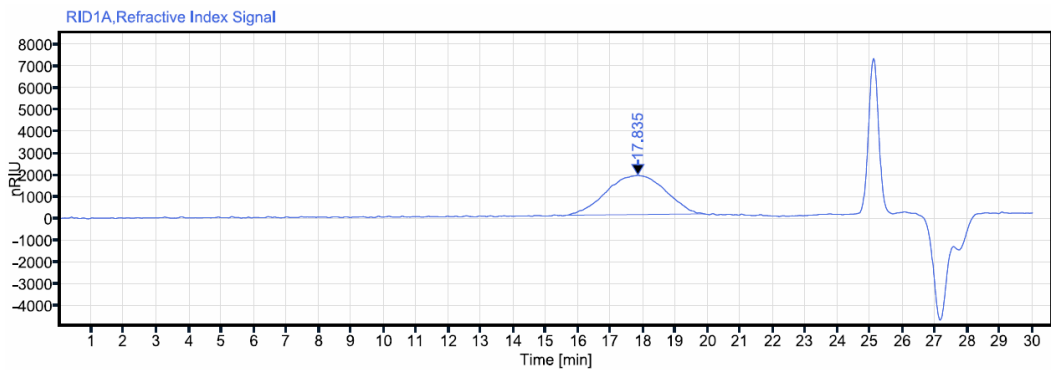


Figure S21. GPC chromatograph of polymer P1.

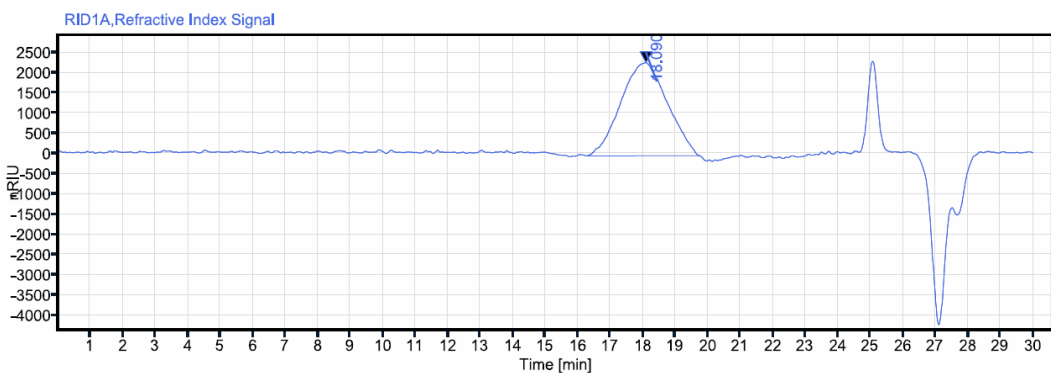
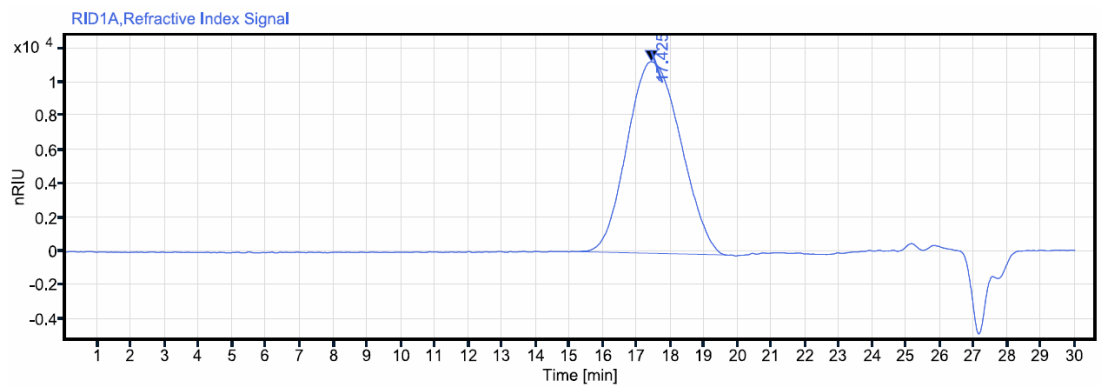


Figure S22. GPC chromatograph of polymer P2.



Peak #	M _p (g/mol)	M _n (g/mol)	M _w (g/mol)	M _z (g/mol)	M _{z+1} (g/mol)	M _v (g/mol)	PD
1	97295	65665	111938	178844	260256	168061	1.704683

Figure S23. GPC chromatograph of polymer P3.

Table S1. Macromolecular, optical, and electrochemical properties of IDTz-DPP based copolymers P1–P3.

Polymer	M_n , ^a (kg mol ⁻¹)	D ^b	λ_{max} , ^c (nm) solution	λ_{max} , ^c (nm) film	λ_{edge} , ^d (nm)	E_g^{opt} , ^e (eV) film	E_{HOMO} , ^f (eV)	E_{LUMO} , ^f (eV)	E_g^{EC} , ^g (eV)
P1	48.5	1.92	729, 669 ^h	740, 671 ^h	787	1.57	-5.26	-3.51	1.75
P2	39.9	2.00	729, 668 ^h	742, 672 ^h	795	1.56	-5.18	-3.38	1.80
P3	65.5	1.70	728, 668 ^h	737, 669 ^h	781	1.59	-5.23	-3.37	1.86

^a Determined by SEC vs polystyrene standards; ^b $D = M_w/M_n$; ^c λ_{max} in a chloroform solution and in a thin film spin coated from chloroform solution on quartz; ^d Onset values of absorption spectra in a thin film; ^e Optical band gap $E_g^{\text{opt}} = 1240/\lambda_{\text{edge}}$; ^f Electrochemical $E_{\text{HOMO}}/E_{\text{LUMO}} = E_{\text{onset}}(\text{Fc}/\text{Fc}^+ \text{ vs. Ag}/\text{Ag}^+) - E_{\text{onset}} - 4.8$, where 4.8 eV is the ferrocene energy level below the vacuum level and $E_{\text{onset}}(\text{Fc}/\text{Fc}^+ \text{ vs. Ag}/\text{Ag}^+) = 0.46$ V; ^g Electrochemical band gap $E_g^{\text{EC}} = E_{\text{HOMO}} - E_{\text{LUMO}}$; ^h Shoulder peak.

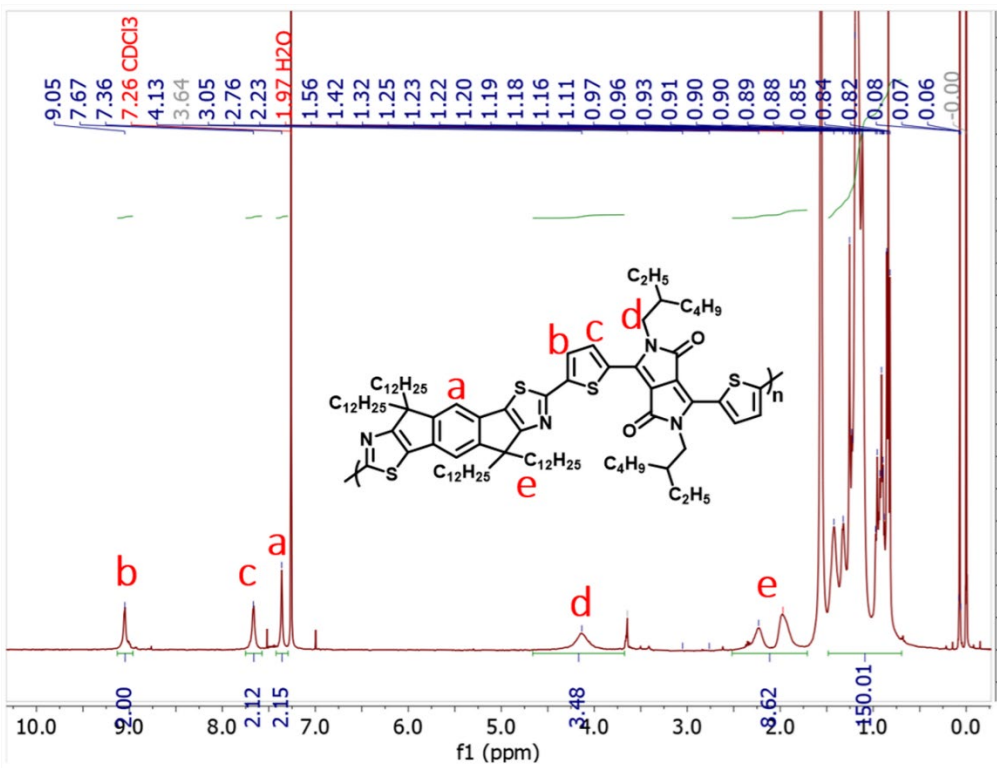


Figure S24. ^1H NMR (CDCl_3 , 400 MHz, 298 K) of polymer P1.

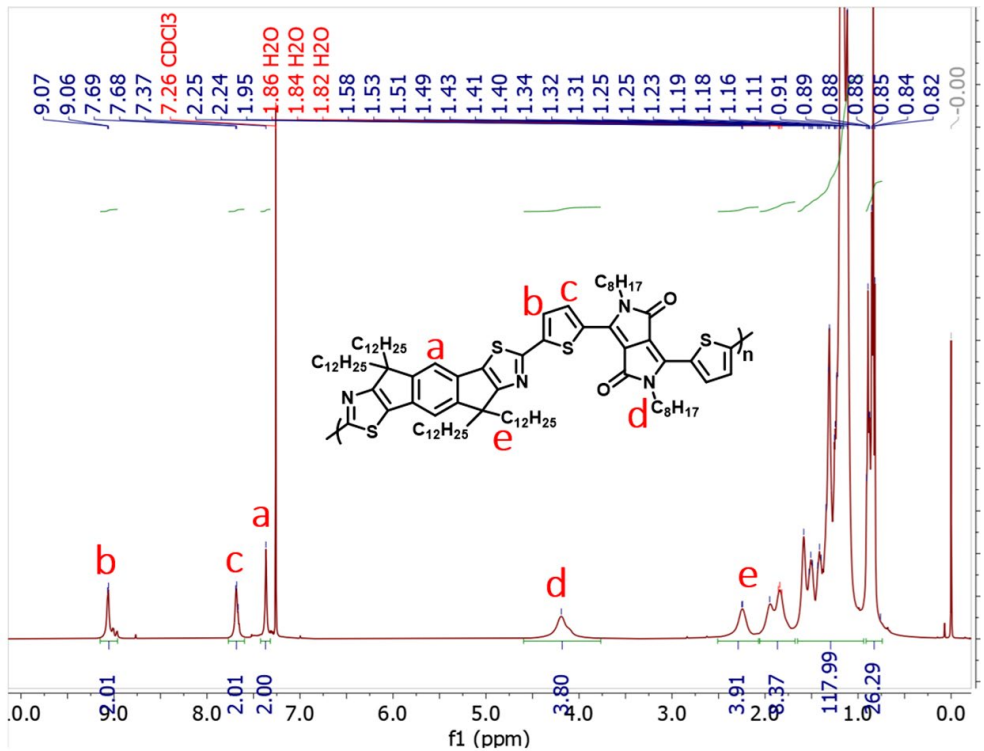


Figure S25. ^1H NMR (CDCl_3 , 400 MHz, 298 K) of polymer P2.

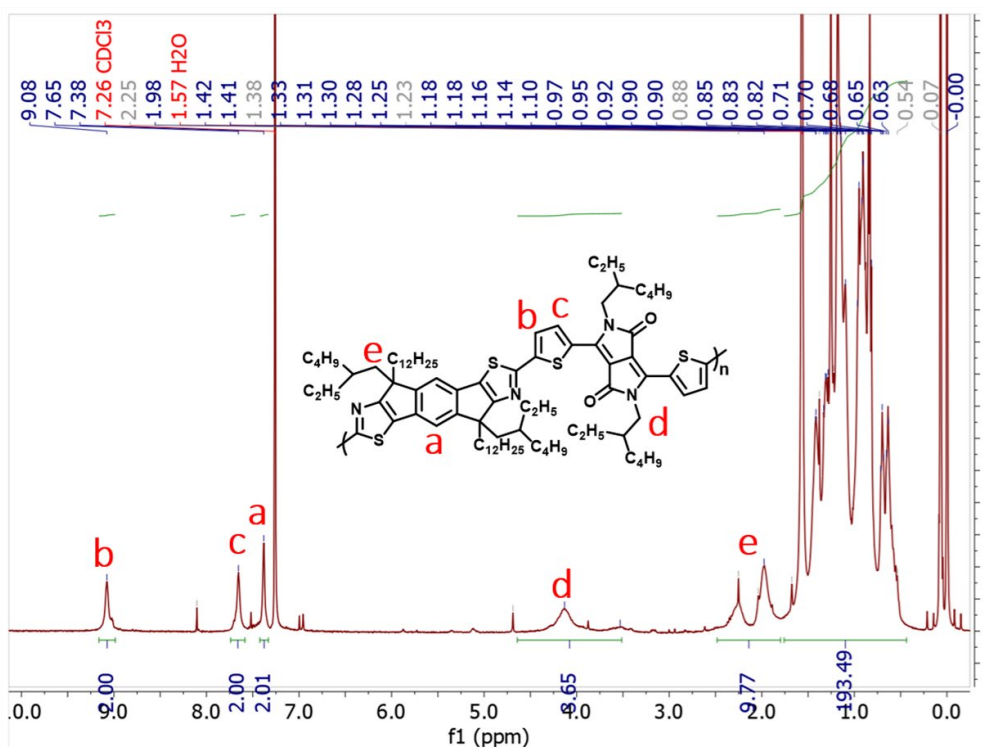


Figure S26. ${}^1\text{H}$ NMR (CDCl_3 , 400 MHz, 298 K) of polymer P3.